



Rapid Loss of CD4 T Cells by Pyroptosis during Acute SIV Infection in Rhesus Macaques

Xuan He,^a Malika Aid,^a John D. Ventura,^a Erica Borducchi,^a Michelle Lifton,^a Jinyan Liu,^a Dan H. Barouch^{a,b}

^aCenter for Virology and Vaccine Research, Beth Israel Deaconess Medical Center, Harvard Medical School, Boston, Massachusetts, USA

^bRagon Institute of MGH, MIT, and Harvard, Cambridge, Massachusetts, USA

ABSTRACT The mechanisms underlying depletion of CD4 T cells during acute HIV-1 infection are not well understood. Here we show that caspase-1-induced pyroptosis, a highly inflammatory programmed cell death pathway, is the dominant mechanism responsible for the rapid depletion of CD4 T cells in gut-associated lymphatic tissue (GALT), spleen, and lymph nodes during acute simian immunodeficiency virus (SIV) infection in rhesus macaques. Upregulation of interferon-gamma inducible factor 16, a host DNA sensor that triggers pyroptosis, was also observed in tissue-resident CD4 T cells and correlated with viral loads and CD4 T cell loss. In contrast, caspase-3-mediated apoptosis and viral cytotoxicity only accounted for a small fraction of CD4 T cell death. Other programmed cell death mechanisms, including mitochondria-induced caspase-independent cell death, necroptosis, and autophagy, did not significantly contribute to CD4 T cell depletion. These data support a model in which caspase-1-mediated pyroptosis is the principal mechanism that results in CD4 T cell loss in the GALT and lymphoid organs and release of proinflammatory cytokines. These findings contribute to our understanding of the pathogenesis of acute SIV infection and have important implications for the development of therapeutic strategies.

IMPORTANCE Different mechanisms for CD4 T cell depletion during acute HIV-1 infection have been proposed. In this study, we demonstrate that in early simian immunodeficiency virus infection, depletion of CD4 T cells is primarily due to pyroptosis. Other mechanisms may also contribute in a minor way to CD4 T cell depletion.

KEYWORDS CD4 T cells, pyroptosis, simian immunodeficiency virus

The precise mechanisms underlying CD4 T cell depletion in acute HIV-1 infection remain unknown. Previous studies have suggested that apoptosis is the main driver of CD4 T cell death during HIV-1 infection using *ex vivo* models (1, 2). However, direct infection of *ex vivo* generated susceptible cells, such as pre-stimulated CD4 T cells or immortalized T cell lines, may bias outcomes in favor of the direct viral cytopathic effects that have been known to induce apoptosis in infected cells (3–7). In contrast, a study using an *ex vivo* human lymphoid aggregate culture (HLAC) system infected with a limited number of HIV virions suggested that pyroptosis, a highly inflammatory form of programmed cell death, was the predominant mode of CD4 T cell death (8). In this study, the majority of CD4 T cell death (~95%) occurred in uninfected bystander cells, and pyroptosis was induced via innate immune sensing of incomplete reverse transcription products accumulated during abortive HIV-1 infection. Additional evidence suggested that cell-to-cell transmission of HIV-1 was critical for activating the pyroptotic pathway, suggesting that infected CD4 T cells rather than free virions were responsible for triggering massive CD4 T cell loss (9). Autophagy, a pathway of cellular degradation independent of caspase-induced cell death, was also reported to occur within bystander CD4 T cells during *ex vivo* HIV-1 infection, contributing to CD4 T cell depletion (10).

The mechanism of systemic CD4 T cell depletion during acute HIV-1 infection *in vivo* remains to be determined. To address this, we evaluated CD4 T cell depletion in

Editor Guido Silvestri, Emory University

Copyright © 2022 He et al. This is an open-access article distributed under the terms of the [Creative Commons Attribution 4.0 International license](https://creativecommons.org/licenses/by/4.0/).

Address correspondence to Dan H. Barouch, dbarouch@bidmc.harvard.edu.

The authors declare no conflict of interest.

Received 20 May 2022

Accepted 4 August 2022

Published 24 August 2022

peripheral blood, spleen, pelvic lymph nodes (LNs), as well as in colon and mesenteric LNs as representatives of gut-associated lymphatic tissue (GALT), which is a major site of viral replication and CD4 T cell depletion after SIV infection (4, 7). By both flow cytometric and transcriptomic analyses of CD4 T cells, we demonstrate that pyroptosis is the predominant mechanism associated with CD4 T cell depletion in peripheral blood, GALT and lymphoid organs during acute SIV infection. Such knowledge contributes to understanding SIV immunopathogenesis and may contribute to the development of novel therapies to improve immunological recovery in HIV-infected patients (11–13).

RESULTS

Pathogenic SIV infection causes rapid loss of CD4 T cells in multiple tissues. To study CD4 T cell dynamics during acute and chronic SIV infection, we conducted a longitudinal study in seven rhesus monkeys infected with SIVmac251. In peripheral blood, median peak plasma viremia occurred on day 14 following SIVmac251 infection, and high-level setpoint viremia persisted in chronic SIV infection as expected (Fig. 1A). To evaluate cellular death pathways occurring within tissue site, we also performed serial necropsies in 19 monkeys at different times following infection, and harvested colon, mesenteric LNs, spleen and pelvic LNs on days 0, 3, 7, and 10 following infection. A nested RT-PCR assay was utilized to quantitate tissue viral RNA levels as described previously (14). All tissues from day 3 following infection were negative for viral RNA (Fig. 1A). In animals necropsied on day 7, we observed wide variations in the levels of viral RNA, about half of which showed detected levels of viral RNA. In contrast, all four animals necropsied on day 10 had high levels of viral RNA ranging from 1×10^7 to 1×10^{10} RNA copies per 10^8 cell equivalents in colon, mesenteric LNs, spleen and pelvic LNs (Fig. 1A). Viral DNA also showed progressive increase in tissues at necropsy from day 3 to day 10 (Fig. S1 in the supplemental material).

We next evaluated the decline of CD4 T cells in blood and tissues during acute SIVmac251 infection. A significant decline of CD4 T cells was observed in peripheral blood by day 14, based on the percentage of CD4 T cells in CD45⁺ leukocytes ($P = 0.004$) (Fig. 1B). The low level of CD4 T cells persisted throughout chronic SIV infection. The absolute number of CD4 T cells in blood also declined progressively in acute SIV infection, with significant decrease on day 56 following SIV challenge ($P = 0.012$) (Fig. 1B). In tissues, the percentage of CD4 T cells in CD45⁺ leukocytes significantly dropped from a mean level of 29.0% on day 0 to 7.4% on day 10 postinfection in colon ($P = 0.005$), from 38.1% to 14.7% in mesenteric LNs ($P = 0.024$), from 23.1% to 6.4% in spleen ($P = 0.008$), and from 42.4% to 18.7% in pelvic LNs ($P = 0.034$) (Fig. 1B). This observation of dramatic loss of CD4 T cells in multiple tissues during acute SIV infection is consistent with previous studies (4, 15).

We next assessed CD4 T cell subpopulations, including naive (CD28⁺/CD95⁻), central memory (CD28⁺/CD95⁺) and effector memory (CD28⁻/CD95⁺) cells based on CD28 and CD95 markers as described previously (15). A significant drop of central memory (CM) CD4 T cells was observed in peripheral blood by day 14 following SIV infection ($P = 0.02$), and naive CD4 T cells were reduced by day 63 ($P = 0.001$) (Fig. 1C). In tissues, the frequency of naive and CM CD4 T cells also declined significantly by day 10 following SIV infection compared to uninfected controls (for naive CD4 in colon, $P = 0.048$; for CM CD4 in colon, $P = 0.004$; for CM CD4 in mLN, $P = 0.038$; for CM CD4 in spleen, $P = 0.02$; for naive CD4 in pLN, $P = 0.042$) (Fig. 1C). In addition, we evaluated the immune status of CD4 T cells in peripheral blood and tissues. We observed an early increase of CD69⁺ CD4 T cells in colon on day 10 following challenge ($P = 0.04$) (Fig. S2A in the supplemental material). In addition, we also observed a significant increase in CD4 T cell proliferation in colon ($P = 0.032$) and in pelvic LNs ($P = 0.047$) by days 7 and 10, respectively (Fig. S2B), suggesting active immunological engagement by CD4 T cells during acute infection. Taken together, this longitudinal study of CD4 T cell dynamics confirmed rapid loss of CD4 T cells in both peripheral blood and tissues following pathogenic SIVmac251 infection.

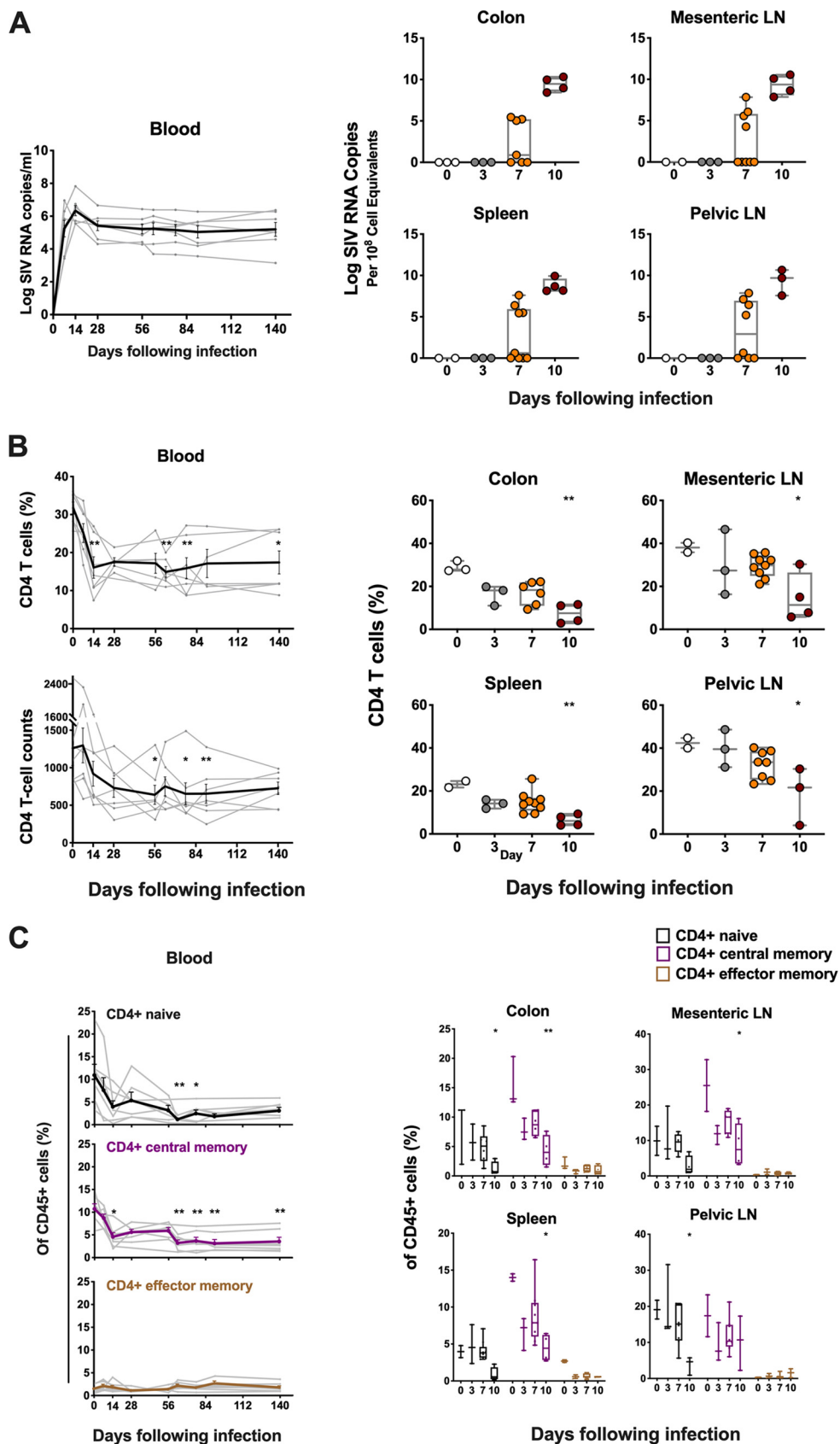


FIG 1 Dynamics of viral RNA and CD4 T cells in blood and tissues. (A) Viral RNA (log RNA copies/mL) in blood in monkeys from day 0 to 140 following inoculation with SIVmac251, and tissue viral RNA (log RNA copies/ 10^8 cell (Continued on next page)

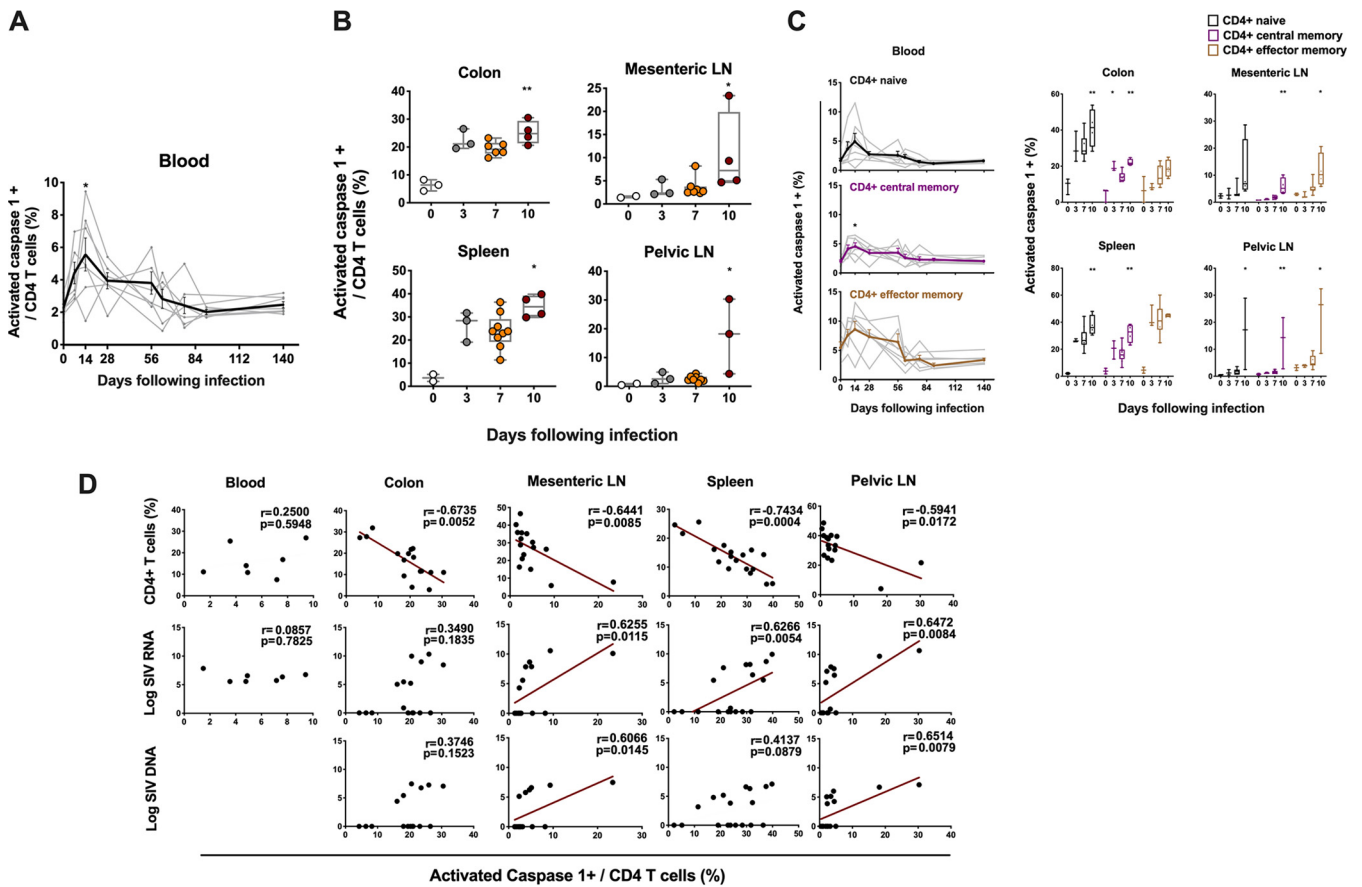


FIG 2 Pyroptosis of CD4 T cells in blood and tissues following SIV infection. (A) The line chart shows pyroptosis of CD4 T cells in blood from seven monkeys at different time points ranging from day 0 to day 140 following SIVmac251 infection. (B) Pyroptosis of CD4 T cells was analyzed by activated caspase 1 staining of CD4 T cells in GALT and lymphoid tissues at necropsy during pathogenic SIVmac251 infection. (C) Pyroptosis of naive and memory CD4 T cell subsets in blood and different tissues at necropsy during pathogenic SIVmac251 infection. Black, purple and brown correspond to naive, central memory and effector memory CD4 T cell subset, respectively. (D) The correlation between the expression of activated caspase 1 in CD4 T cells and the percentage of CD4 T cells or the magnitude of viral RNA or DNA in blood on day 14 and in multiple tissues from all the SIV-infected monkeys at necropsy. Solid lines indicate the correlation with significant *P* values. Significant *P* values are shown in figures. Experimental variables were analyzed by one-way analysis of variance (ANOVA). *, *P* < .05; **, *P* < .01. For correlation analysis, spearman rank order correlation coefficients *r* and corresponding *P* values are indicated.

CD4 T cell depletion in GALT and secondary lymphoid tissues is strongly associated with pyroptosis. We next evaluated the potential mechanisms of CD4 T cell depletion. Activated caspase 1, a marker commonly used for pyroptosis (8), was detected longitudinally in peripheral blood and tissues. Peripheral blood CD4 T cells showed a modest increase of activated caspase 1 during acute SIV infection, which peaked on day 14 to a mean level of 5.5% following infection (*P* = 0.03 compared to day 0) (Fig. 2A; Fig. S3A in the supplemental material). In contrast, there was a dramatic increase of CD4 T cell pyroptosis observed on day 10 following challenge in multiple tissues, to a mean level of 25.1% in colon (*P* = 0.007), 10.6% in mesenteric LNs (*P* = 0.01), 34.6% in spleen (*P* = 0.01), and 17.6% in pelvic LNs (*P* = 0.01) (Fig. 2B; Fig. S3B).

We also assessed pyroptosis of CD4 T cells by evaluating the magnitude of activated caspase 1 in naive and memory CD4 T cell compartments in blood and tissues. Generally, lower

FIG 1 Legend (Continued)

equivalents) in multiple tissues at necropsies in monkeys on days 0, 3, 7 or 10 following SIVmac251 infection. (B) Percentage and absolute number of CD4 T cells in blood and in multiple tissues at necropsy in monkeys with SIVmac251 infection at different time points. (C) The dynamics of CD4 T cell naive and memory subsets in blood and different tissues during pathogenic SIVmac251 infection. Black, purple and brown correspond to naive, central memory and effector memory CD4 T cell subset, respectively. Significant *P* values are shown in figures. Experimental variables were analyzed by one-way analysis of variance (ANOVA). *, *P* < .05; **, *P* < .01.

expression of caspase 1 was found in CD4 naive and memory cells in blood compared to tissues (Fig. 2C). Increased pyroptotic activity was observed in CD4 naive subset in most tissues as early as day 10 (for colon, $P = 0.009$; for spleen, $P = 0.008$; for pelvic LNs, $P = 0.013$). CD4 CM cells showed increased pyroptosis in blood on day 14 ($P = 0.035$), and in GALT and lymphoid tissues on day 10 following infection (for colon, $P = 0.003$; for mesenteric LNs, $P = 0.004$; for spleen, $P = 0.005$; for pelvic LNs, $P = 0.008$). Although we did not detect an obvious decline in CD4 effector memory (EM) cells which are a small subpopulation of CD4 T cells in blood and tissues, an increase in pyroptotic activity was observed in EM CD4 cells, reaching significance in mLN ($P = 0.045$) and pLN ($P = 0.03$) during early SIV infection (Fig. 2C).

We next assessed whether CD4 T cell pyroptosis was associated with CD4 T cell depletion and viral RNA or DNA in blood and tissues during early SIV infection. CD4 T cell pyroptosis showed a strong negative correlation with CD4 T cells from different tissues evaluated, including colon ($r = -0.67$, $P = 0.005$), mesenteric LNs ($r = -0.64$, $P = 0.008$), spleen ($r = -0.74$, $P = 0.0004$) and pelvic LNs ($r = -0.59$, $P = 0.01$). CD4 T cell pyroptosis was also positively correlated with viral RNA in mesenteric LNs ($r = 0.62$, $P = 0.01$), spleen ($r = 0.62$, $P = 0.005$), and pelvic LNs ($r = 0.64$, $P = 0.008$) and was associated with viral DNA in mesenteric LNs ($r = 0.60$, $P = 0.01$) and pelvic LNs ($r = 0.65$, $P = 0.007$) (Fig. 2D). Additionally, the level of naive CD4 T cells showed significantly negative correlations with its pyroptotic activity in colon ($r = -0.66$, $P = 0.004$) and pelvic LNs ($r = -0.56$, $P = 0.02$), and percentage of CM CD4 T cells was also highly associated with its pyroptosis in colon ($r = -0.76$, $P = 0.0006$), mesenteric LNs ($r = -0.59$, $P = 0.01$) and spleen ($r = -0.83$, $P < 0.0001$) (Fig. S3C in the supplemental material). Furthermore, CCR5 expression in CD4 T cells was correlated with pyroptosis of CD4 T cells in colon ($r = 0.91$, $P < 0.0001$) (Fig. S3D). Taken together, these data suggest that pyroptosis was highly associated with reduced CD4 T cells, including naive and central memory CD4 T cells, and was correlated with levels of viral RNA in lymphoid organs during early SIV infection.

SIV-mediated apoptosis was only minimally detected in CD4 T cells during acute SIV infection. Multiple reports have suggested increased apoptosis of CD4 T cells during SIV infection (4, 16, 17). To evaluate the contribution of apoptotic activity to CD4 T cell death, we investigated the kinetics of CD4 T cell apoptosis via flow-cytometric detection of intracellular activated caspase 3, a well-characterized effector marker of apoptosis (8, 16). There was a detectable but marginal increase of CD4 T cells expressing caspase 3 on day 14 compared to day 0 in peripheral blood during early SIV infection ($P = 0.008$) (Fig. 3A; Fig. S4 in the supplemental material). In tissues, modest increases of caspase 3 expression in CD4 T cells were also observed by day 10 following SIVmac251 infection in colon ($P = 0.04$) and spleen ($P = 0.03$) with less than 4% tissue-resident CD4 T cells undergoing apoptosis (Fig. 3B; Fig. S4B). No obvious change of caspase-3 expression was observed in CD4 T cell naive or memory compartments in tissues during early SIV infection (Fig. 3C). CD4 T cell apoptosis was negatively correlated with percentage of CD4 T cells from colon ($r = -0.60$, $P = 0.01$) and mesenteric LNs ($r = -0.63$, $P = 0.004$) (Fig. 3D). Notably, in contrast with caspase-1-mediated pyroptosis, caspase-3-mediated apoptosis was positively correlated with viral RNA in colon ($r = 0.68$, $P = 0.004$). In general, caspase-3-mediated apoptosis accounted for <4% of CD4 T cell death in GALT and lymphoid organs.

Other programmed cell death mechanisms contribute minimally to CD4 T cell depletion. We next performed a longitudinal transcriptomic analysis of sorted CD4 T cells in mesenteric and pelvic lymph nodes between day 0 and day 10 via bulk RNA-seq. We observed a significant increase of the number of reads mapped to the SIV genome on day 10 in total RNA extracted from CD4 T cells in LNs ($P < 0.05$) (Fig. S5 in the supplemental material), indicating the presence of productive SIV within CD4 T cells following infection. The number of reads mapped to SIV were also associated with viral loads ($r = 0.66$, $P = 0.00005$) and CD4 T cells ($r = -0.58$, $P = 0.00056$) as expected (Fig. S5). To evaluate the direct impact of SIVmac251 infection on CD4 T cell death, we quantified the percentage of CD4 T cells containing SIV transcripts. A flow cytometry-based assay capable of measuring SIV transcription in CD4 T cells

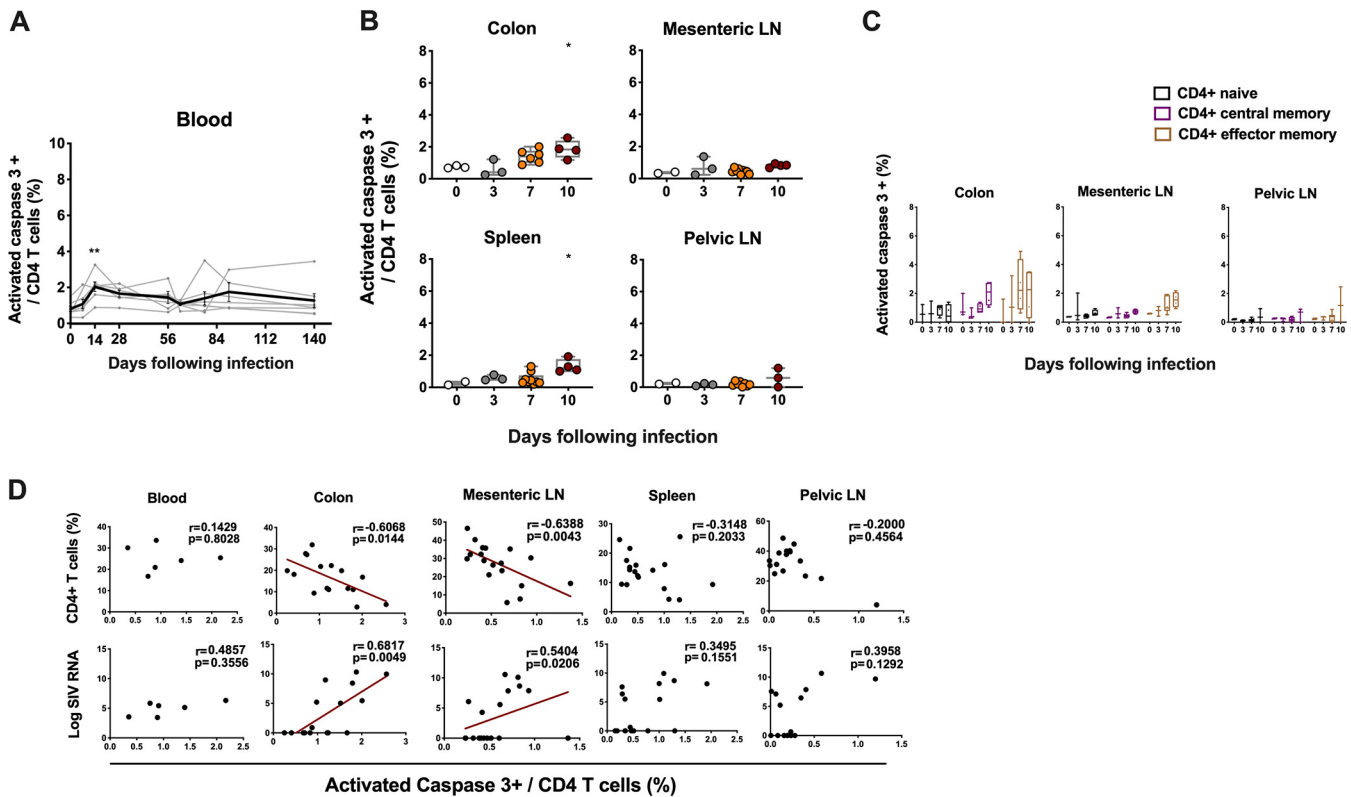


FIG 3 Apoptosis of CD4 T cells in blood and tissues following SIV infection. (A) The line chart shows apoptosis of CD4 T cells in blood from seven monkeys at different time points ranging from day 0 to day 140 following SIVmac251 infection. (B) Apoptosis of CD4 T cells was analyzed by activated caspase 3 staining of CD4 T cells in multiple tissues at necropsy during pathogenic SIVmac251 infection. (C) The apoptosis of naive, central memory (CM) and effector memory (EM) CD4 T cell subsets in colon, mesenteric or pelvic LNs during pathogenic SIVmac251 infection. Black, purple and brown correspond to naive, CM and EM CD4 T cell subset, respectively. (D) The correlation between the expression of activated caspase 3 in CD4 T cells and the percentage of CD4 T cells or the magnitude of viral RNA in blood on day 14 and in multiple tissues from all the SIV-infected monkeys at necropsy. Solid lines indicate the correlation with significant *P* values. Significant *P* values are shown in figures. Experimental variables were analyzed by one-way analysis of variance (ANOVA). *, *P* < .05; **, *P* < .01. For correlation analysis, spearman rank order correlation coefficients *r* and corresponding *P* values are indicated.

undergoing infection was utilized. During early SIV infection in monkeys, less than 0.5% of CD4 T cells in peripheral blood exhibited productive SIV infection (Fig. 4A). Higher frequencies of SIV+ CD4 T cells were observed in lymphoid tissues on day 10 following SIV infection, but still <5% of CD4 T cells (Fig. 4A). As expected, SIV-infected CD4 T cells from blood or tissues resided in CD95+ memory subsets with high levels of CCR5 expression (Fig. S6). Considering that more than 95% of CD4 T cells were negative for SIV-associated transcripts and yet we detected on average 10~35% of the entire CD4 T cell population expressing activated caspase 1 in tissues, it suggested that the vast majority of caspase-1-expressing pyroptotic cells during acute SIV infection were nonproductively infected bystander cells.

Caspase-independent cell death (CICD) is an apoptotic pathway that does not include executioner caspase activation (e.g., caspase 1, 3, and 11) (18–20). HIV-1 Vpr has been reported to kill cells by this pathway, in which mitochondrial membrane permeabilization was involved as a crucial step (21). *BCL2L14* and *BAK1*, which both belong to the *Bcl-2* gene family and are capable of regulating apoptotic pathway via mitochondria (22), were upregulated in CD4 T cells from mesenteric LNs (*BCL2L14*, *P* = 0.01; *BAK1*, *P* = 0.009) and pelvic LNs (*BCL2L14*, *P* = 0.02; *BAK1*, *P* = 0.04) on day 10 following SIV infection by transcriptomic profiling. These data suggested activation of mitochondria in LN-resident CD4 T cells during early SIV infection. In addition, based on flow cytometric and transcriptomic analyses, we did not observe the downstream activation of executioner caspases, which suggested the possibility of mitochondria-induced CICD in CD4 T cells that may be contributing to CD4 T cell depletion during early SIV infection. We therefore checked the proportion of CD4 T cells with CICD-associated

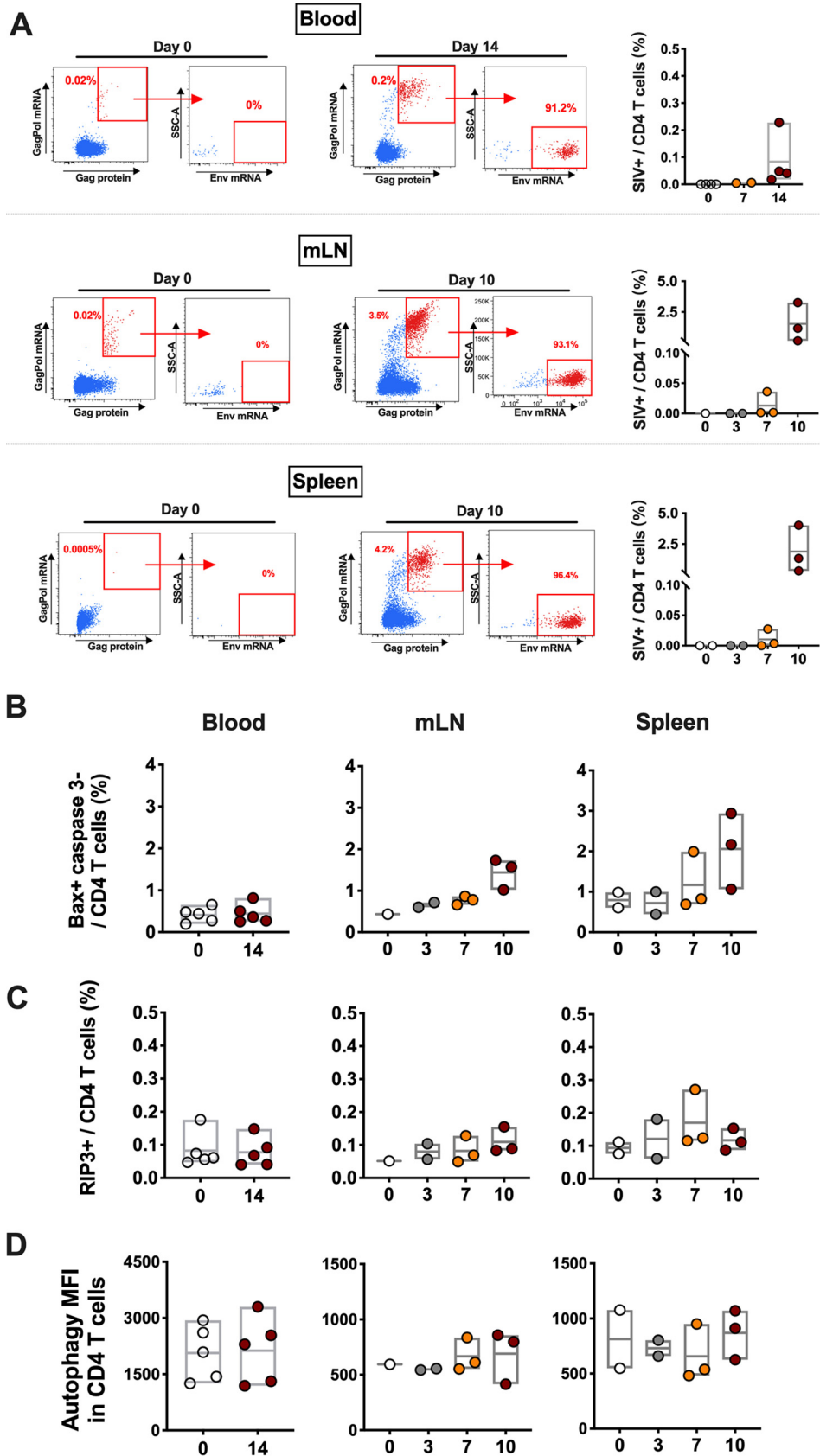


FIG 4 Quantification of SIV-infected CD4 T cells with translation-competent virus, and mitochondria-induced caspase-independent cell death, necroptosis or autophagy of CD4 T cells in blood and tissues. (A) Representative (Continued on next page)

gene expression in blood or tissues from SIV-infected monkeys. Bax protein, which is essential in triggering permeabilization of mitochondria (23), was introduced in the flow cytometric analyses. As expected, CD4 T cells undergoing apoptosis expressed both Bax and caspase 3 (Fig. S7A in the supplemental material). Of note, we observed the CD4 T cell populations with Bax expression but negative for caspase 3 which were qualified for carrying out mitochondria-induced CICD. However, no significant changes regarding the percentage of Bax⁺ caspase 3⁻ CD4 T cells were observed in blood, spleen and mLN during the course of early infection (Fig. 4B). To account for additional cell death possibilities, we assessed the role of necroptosis and autophagy during early SIV infection. Receptor interacting protein 3 (RIP3), a marker for necroptosis (24), was assessed in CD4 T cells from blood and lymphoid tissues. Less than 0.5% of CD4 T cells expressing RIP3 proteins were observed in blood or tissues, and RIP3⁺ CD4 T cells stayed at low level during early SIV infection (Fig. 4C; Fig. S7B). Although HIV Env-mediated autophagy was found in CD4 T cells in HIV infection when apoptosis was blocked (10), we did not observe any significant changes regarding autophagy of CD4 T cell population during early SIV infection (Fig. 4D; Fig. S7C).

Transcriptional changes in CD4 T cells during early SIV highlight potent pyroptotic activity of CD4 T cells. To further elucidate the mechanistic basis of CD4 T cell depletion following early SIV infection, we evaluated transcriptional profiling of CD4 T cells from mesenteric and pelvic lymph nodes following SIV infection by bulk RNA-seq. Approximately 1000 genes were captured and showed significant changes in CD4 T cells from mesenteric LNs (mLNs) and pelvic LNs (pLNs) on day 10 following infection compared to uninfected controls, of which 493 genes showed significant differential expression in both mLNs and pLNs (Fig. 5A). Gene set enrichment analysis (GSEA) revealed significant enhancement of interferon (mLNs, NES = 3.13, FDR q value < 10⁻⁶; pLNs, NES = 3.21, FDR q value < 10⁻⁶) and inflammatory response pathways (mLNs, NES = 2.63, FDR q value < 10⁻⁶; pLNs, NES = 2.72, FDR q value < 10⁻⁶) in CD4 T cells on day 10 following infection compared to uninfected controls (Fig. 5B). Transcriptomic analyses showed further evidence of SIV replication in CD4 T cells, as shown by upregulation of HIV infection pathways (mLNs, NES = 1.38, FDR q value = 0.02; pLNs, NES = 1.55, FDR q value = 0.02) (Fig. 5B).

Of importance, GSEA reported an induction of pyroptotic signaling in CD4 T cells from both mLNs and pLNs on day 10 following SIV infection (Fig. 5B–D). Consistent with the flow cytometric analysis, caspase 1 gene *CASP1* was significantly upregulated in CD4 T cells from mLNs ($P = 0.00002$) and pLNs ($P = 0.0006$) on day 10 compared with day 0 based on gene expression analysis. We also observed upregulation of *CASP4* in mLNs ($P = 0.0001$) and pLNs ($P = 0.0004$). It has been reported that caspase 4 may trigger activation of caspase 1 in macrophages during dengue infection (25). Previous reports have also identified interferon-gamma-inducible protein 16 (IFI16) as a key inflammasome DNA sensor, thus making IFI16 an important component in the canonical pyroptotic pathway (26). *IFI16* was strongly upregulated in CD4 T cells from mLNs ($P = 0.000009$) and pLNs ($P = 0.001$) on day 10 following SIV infection (Fig. 5C, D). Gasdermin D (*GSDMD*), an executor of pyroptosis, was observed with trend of upregulation on day 10 ($P = 0.08$), and was highly associated with viral loads ($r = 0.64$, $P = 0.000054$) in LNs. The proinflammatory cytokines *IL-16* and *TNF* as well as the receptor genes for inflammatory cytokine receptors including *IL6ST*, *IL15RA*, *IL18R1* were upregulated in CD4 T cells from lymph nodes on day 10 following infection compared to uninfected controls (*IL-16* in mLNs, $P = 0.02$; *TNF* in mLNs, $P = 0.04$; *IL6ST* in mLNs,

FIG 4 Legend (Continued)

flow cytometric plots showing CD4 T cells with or without translation-competent SIV in blood on day 0 or day 14 following infection, as well as in mesenteric LNs and spleen on day 0 or day 10 following infection. In the summary figures, CD4 T cells with productive SIV infection were quantified in blood on days 0 and 14, and in mesenteric LNs and spleen on days 0, 3, 7, or 10 during SIVmac251 infection. (B) CD4 T cells undergoing mitochondria-induced caspase-independent cell death were analyzed in blood and tissues during SIVmac251 infection. (C) CD4 T cells undergoing necroptosis were analyzed in blood and tissues during SIVmac251 infection. (D) CD4 T cells undergoing autophagy were analyzed in blood and tissues during SIVmac251 infection.

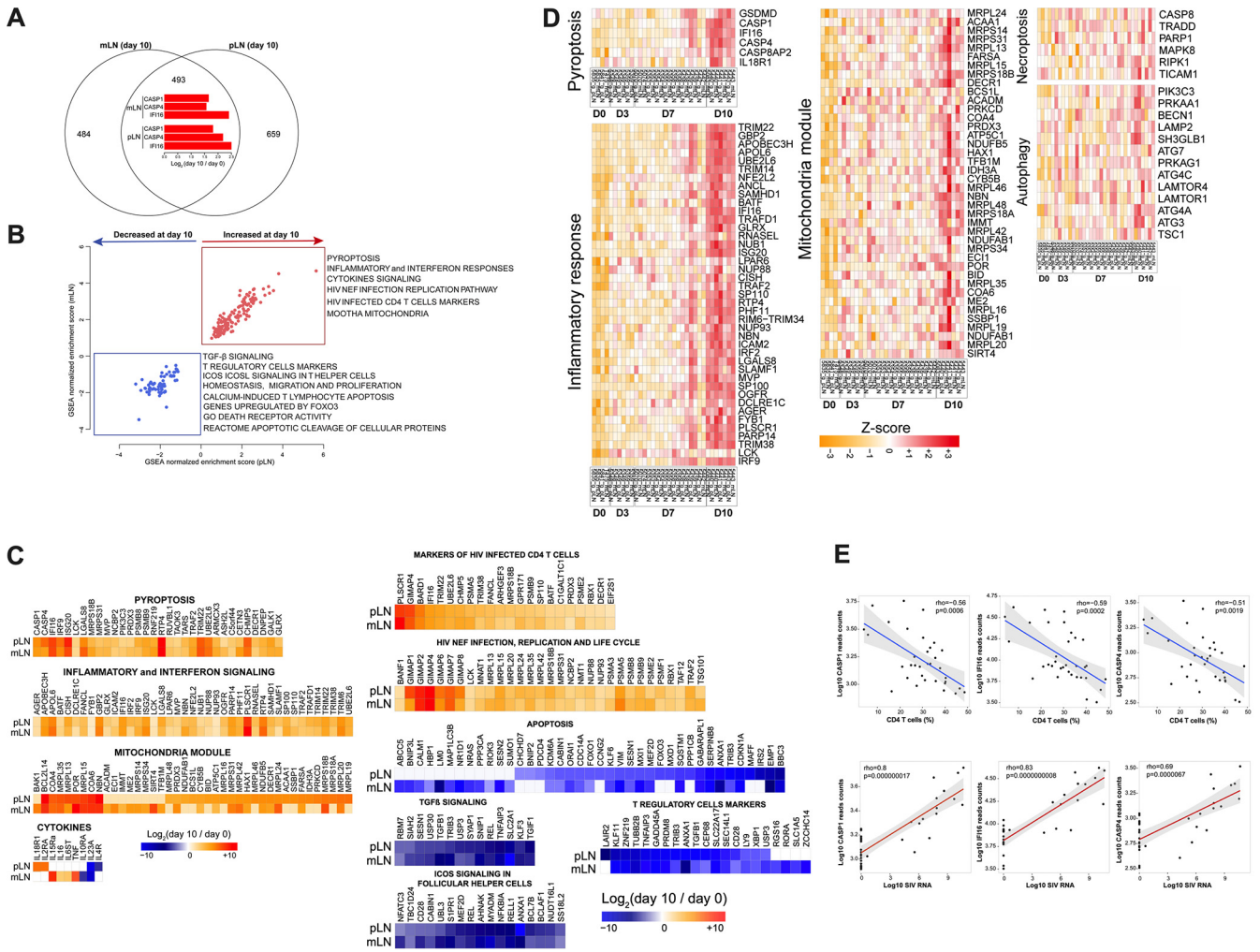


FIG 5 Pyroptosis and inflammatory signaling in sorted CD4 T cells from mesenteric LNs and pelvic LNs from SIV-infected monkeys. (A) Venn diagram (top) of genes significantly increased or decreased at day 10 compared to day 0 in sorted CD4 T cells from mesenteric LN (mLN) and pelvic LN (pLN) in SIV-infected monkeys. All genes with a BH-corrected *P* of 0.05 were selected (493 common genes, 484 genes unique to mLN and 659 unique to pLN). The common plot area exhibited barplots of the log₂ fold change expression (day10/day 0) of pyroptotic markers *CASP1*, *CASP4* and *IFI16* in mLN and pLN. (B) The scatterplots represent the normalized enrichment score (NES) of the top enriched pathways at day 10 compared to day 0 in mLN and pLN. Pathways increased at day 10 were represented in red and pathways decreased at day 10 were represented in blue dots, where each dot corresponds to an individual pathway. *x* axis represents the pathways NES in pLN and *y* axis the pathways NES in mLN. Each dot on the plot represents a pathway, where increased pathways are represented in red dots and decreased pathways are represented in blue dots. (C) Heatmaps showing the log₂ fold change (day 10/day 0) of the significant genes in pathways. Color gradients represent the log₂ fold change ranging from blue (decreased) to white (not significant) to red (increased). All genes were selected using a BH-corrected *P* of 0.05. (D) Heatmaps of the row scaled normalized-expression of markers of pyroptosis, inflammatory response, mitochondria module, necroptosis, autophagy. Each column represents an individual animal separated by time points. Each row represents an individual gene. Heatmap color gradient represent the Z-score scaled expression of genes at days 0, 3, 7 and 10, ranging from yellow (decreased) to white (not significant) to red (increased). Animals are grouped by time points as follow: baseline (day 0) and following infection (days 3, 7, 10). (E) Scatterplots of the log transformed expression of pyroptotic markers *CASP1*, *IFI16*, *CASP4* correlated with the frequency of CD4 T cells (top) and viral RNA (bottom) at days 0, 3, 7 and 10 following SIV infection. Spearman correlation coefficient (ρ) and *P* value are shown for each gene. Gray area represents the confidence interval (CI) of 95%.

P = 0.007; *IL15RA* in mLNs, *P* = 0.01; *IL18R1* in pLNs, *P* = 0.03) (Fig. 5C). We also checked genes that are relevant to other cell death pathways including apoptosis, autophagy, and necroptosis in CD4 T cells from lymph nodes, and transcriptomic profiling revealed no significant upregulation of these pathways (Fig. 5C, D).

Expression of these genes associated with pyroptosis, including *CASP1*, *CASP4* and *IFI16*, were inversely correlated with CD4 T cell level (*CASP1*, *r* = -0.56, *P* = 0.0006; *IFI16*, *r* = -0.59, *P* = 0.0002; *CASP4*, *r* = -0.51, *P* = 0.0019) and were positively correlated with viral loads in these animals (*CASP1*, *r* = 0.80, *P* < 0.0001; *IFI16*, *r* = 0.83, *P* < 0.0001; *CASP4*, *r* = 0.69, *P* < 0.0001) (Fig. 5E). Genes associated with inflammatory pathways were also highly associated with CD4 T cell frequency and viral loads in the

macaques (Fig. S8 in the supplemental material). Taken together, these data demonstrate upregulation of genes involved in the pyroptotic pathway in SIV-infected rhesus macaques, consistent with the flow cytometric studies, suggesting that pyroptosis plays a key role in CD4 T cell depletion during acute SIV infection.

DISCUSSION

This study extends prior *ex vivo* studies (8, 9) and provides comprehensive *in vivo* evidence that pyroptosis is the predominant mechanism of systemic CD4 T cell depletion in SIV-infected rhesus macaques. Pyroptosis of CD4 T cells was observed by both flow cytometry and transcriptomics and was particularly evident in GALT and lymphoid tissues (4, 27).

Our results confirm and extend a previous study showing upregulation of genes involved in pyroptosis pathway in draining LNs during early SIV infection by bulk RNA-seq (28). We investigated immunologic and transcriptomic profiles of systemic CD4 T cells from GALT and lymphoid tissues during acute SIV infection and assessed the contributions from all potential programmed cell death mechanisms to CD4 T cell death. Our data suggest that the pyroptosis of CD4 T cells was the dominant mode responsible for CD4 T cell loss either in GALT or lymphoid tissues. In addition, we observed lower pyroptosis of CD4 T cells in peripheral blood compared with lymphoid tissues, consistent with a previous report showing that blood CD4 T cells are partially resistant to pyroptosis due to deeper resting state with less DNA sensor IFI16 (29). Moreover, CD4 T cells in lymphoid tissues with higher proportions of SIV infection may facilitate pyroptosis of surrounding bystander CD4 T cells by cell-to-cell interactions (9). Our transcriptomic data also highlight the potential role of IFI16, an HIV-1 DNA sensor which leads to caspase 1 activation. During early HIV or SIV infection, IFI16 is able to detect viral DNA transcripts and triggers inflammasome assembly, which then leads to activation of caspase 1 and trigger pyroptosis in CD4 T cells.

The study of HIV-1 infection using HLAC system highlighted the massive death caused by pyroptosis occurring in bystander CD4 T cells (8). During SIV infection, we observed profound depletion of naive CD4 T cells derived from tissues and associated with pyroptosis. The depletion of naive CD4 T cell populations provides indirect evidence for a strong bystander effect, especially within the gastrointestinal tract and other tissue compartments. Moreover, the drastic loss of naive or central memory CD4 T cells causes the insufficient generation and delivery of CD4 T cell effectors fighting against SIV infection and leads to onset of progressive SIV pathogenesis.

In contrast with pyroptosis, we observed only a small proportion of CD4 T cells expressing caspase 3, indicative of minimal apoptosis of CD4 T cells in peripheral blood and tissues during early SIV infection. Our data are consistent with the *ex vivo* study using the HLAC system (8), suggesting that apoptosis-mediated CD4 T cell death may be a minor component of CD4 T cell depletion *in vivo*. Moreover, the low frequency of CD4 T cells undergoing productive SIV infection in blood and tissues indicate that direct virus cytotoxicity provides only minimal contribution to CD4 T cell loss. Another *ex vivo* study has observed that the activation of DNA-dependent protein kinase (DNA-PK) contributes to CD4 T cell death during the process of viral integration (3). In our study, no obvious change regarding gene expression of DNA-PK was observed in CD4 T cells. Moreover, other programmed cell death pathways including autophagy, necroptosis and mitochondria-induced CICD appeared to barely play roles in CD4 T cell depletion during acute SIV infection.

Taken together, our observations show that CD4 T cell depletion in acute SIV infection in rhesus macaques is primarily the result of caspase-1-mediated pyroptosis. These findings have important implications for our understanding of HIV-1 pathogenesis and may provide new therapeutic targets for immunological recovery.

MATERIALS AND METHODS

Animals and infections. Twenty-six outbred, Indian-origin adult or juvenile female or male rhesus monkeys (*Macaca mulatta*) were genotyped and selected as negative for the protective MHC class I

alleles Mamu-A*01, Mamu-B*08, and Mamu-B*17. TRIM5 polymorphisms were balanced equally among groups, and animals were otherwise randomly allocated. All monkeys were housed at Bioqual, Rockville, MD. Nineteen animals were infected with 5×10^4 TCID50 of our SIVmac251 challenge stock by the intravaginal route (14) and were necropsied at time points following infection. Multiple frozen tissues including colon ($n = 3$ for day 0; $n = 3$ for day 3; $n = 7$ for day 7; $n = 4$ for day 10), spleen ($n = 2$ for day 0; $n = 3$ for day 3; $n = 9$ for day 7; $n = 4$ for day 10), mesenteric lymph nodes ($n = 2$ for day 0; $n = 3$ for day 3; $n = 9$ for day 7; $n = 4$ for day 10), and pelvic lymph nodes ($n = 2$ for day 0; $n = 3$ for day 3; $n = 8$ for day 7; $n = 3$ for day 10) were obtained for this study. Another seven monkeys were infected with SIVmac251 challenge stock by intrarectal route, and blood were collected at multiple time points from day 0 to day 140. All animal studies were approved by the appropriate Institutional Animal Care and Use Committee (IACUC).

Viral RNA and DNA. Plasma SIV RNA levels were detected using a *gag*-targeted quantitative real-time RT-PCR assay, and levels of SIV RNA or DNA in tissues were measured using *gag*-targeted, nested quantitative hybrid real-time/digital RT-PCR and PCR assays as previously described (14).

Whole-blood lymphocyte count assay. One hundred microliters of whole blood were stained with monoclonal antibodies CD3 (V450 conjugate), CD4 (PE conjugate) and CD8 (FITC conjugate), then lysed in TQ-Prep and fixed. The acquisitions were performed on LSRFortessa, and flow cytometric analysis was performed by FlowJo software to generate the percentage of CD4 T cells within lymphocytes. Eight hundred microliters of whole blood was obtained from animals and complete blood count performed on Siemens Advia 120. CD4 T cell count was determined by combining cell counts of lymphocytes with the frequency results generated by flow cytometry.

Flow cytometric analysis. The LIVE/DEAD Fixable Aqua Dead Cell Stain Kit was applied to excluding the dead cells. Cell surface staining was conducted using the following monoclonal antibodies including CD45 (BV605 conjugate, clone D058-1283, BD Pharmingen), CD3 (Alexa 700 conjugate, clone SP34.2, BD Pharmingen), CD4 (BB700 conjugate, clone L200, BD Pharmingen), CD8 (Pacific Blue conjugate, clone RPA-T8, BD Pharmingen), CD95 (BV711 conjugate, clone DX2, BD Pharmingen), CD28 (PE-Cy7 conjugate, clone 28.2, ThermoFisher), CD69 (ECD conjugate, clone TP1.55.3, Beckman Coulter), and CD195 (BV650 conjugate, clone 3A9, BD Pharmingen). For intracellular staining, cells were permeabilized using Caltag Fix & Perm (Invitrogen), then stained with monoclonal antibodies including Ki67 (PE conjugate, clone B56, BD Pharmingen) and caspase 3 (BUV395 conjugate, clone C92-605, BD Pharmingen). Fluorescent labeled inhibitor probe FAM-YVAD-FMK (ImmunoChemistry Technologies) which could covalently bind to the activated caspase 1, was applied to detecting the cells containing activate caspase 1. Autophagy probe (ImmunoChemistry Technologies) which fluoresces red when inserting into the lipid membrane of autophagosomes and autolysosomes was applied in the study. After staining, cells were washed and fixed by 2% paraformaldehyde. All data were acquired on BD LSRII flow cytometer and analyzed by FlowJo software (version 9.9.5).

Transcriptomic analysis. CD4 T cells from mesenteric LNs and pelvic LNs in monkeys necropsied on day 0, 3, 7 and 10 following infection were enriched by negative selection through EasySep Non-Human Primate Custom Enrichment Kit (STEMCELL Technologies). The enriched cells were further sorted by BD FACSAria flow cytometer. RNA extraction was carried out using RNeasy minikit (Qiagen) according to manufacturer's instructions. A Low-Input mRNA library (Clontech SMARTer) v4 was applied and samples were sequenced on Illumina NS500 Paired-End 75 bp (PE75) at the Molecular Biology Core Facility at Dana-Farber Cancer Institute. All samples were processed using an RNA-Seq pipeline implemented in the bcbio-nextgen project (<https://bcbio-nextgen.readthedocs.org/en/latest/>). Raw reads were examined for quality issues using FastQC (<http://www.bioinformatics.babraham.ac.uk/projects/fastqc/>) to ensure library generation and sequencing are suitable for further analysis. Adapter sequences, other contaminant sequences such as polyA tails and low-quality sequences with PHRED quality scores less than five were trimmed from reads using atropos (<https://github.com/jdidion/atropos>). Trimmed reads were aligned to the *Macaca mulatta* genome (<https://www.unmc.edu/rhesusgenomechip/index.htm>) using STAR v2.7.3. Alignments will be checked for evenness of coverage, rRNA content, genomic context of alignments (for example, alignments in known transcripts and introns), complexity and other quality checks using a combination of FastQC, Qualimap and other custom tools. Counts of reads aligning to known genes are generated by featureCounts. We used DESeq2 (Moderated estimation of fold change and dispersion for RNA-Seq data with DESeq2) internal filtering algorithm called "independentFiltering" that sets a threshold on the mean of normalized counts of all samples ($\text{baseMean} > 10$) to maximize the number of tests that pass multiple test correction. A corrected P value cut-off 0.05 was used to assess significant genes that were upregulated or downregulated on days 3, 7, and 10 using an adjusted P of < 0.05 and the Benjamini-Hochberg (BH) correction method. Gene set enrichment analysis (30, 31) and database of biological and immunological modules (<https://www.gsea-msigdb.org/gsea/index.jsp>) were used to explore enriched pathways at days 3, 7 and 10 after infection. An FDR q value cut-off 0.05 was used to selected increased or decreased pathways at days 3, 7 and 10 compared to day 0. Raw fastq files were uploaded to NCBI Gene Expression Omnibus (GEO) database under identifier [GSE165519](https://www.ncbi.nlm.nih.gov/geo/query/acc.cgi?acc=GSE165519).

Mapping of SIV RNA. To test for the presence of SIV RNA at days 3, 7 and 10 following SIVmac251 infection, unmapped reads that did not align to the rhesus genome by STAR aligner were extracted and mapped to the SIVmac251 genome using Burrows-Wheeler Aligner bwa mem (<https://github.com/lh3/bwa>).

SIV RNA-Flow FISH. Prior to SIV mRNA detection, cells were stained with viability dye, then surface staining were performed to identify phenotype of cell populations using following monoclonal antibodies including CD45 (BV786 conjugate), CD4 (BB700 conjugate), CD3 (BV421 conjugate), CD195 (BV650 conjugate), CD8 (APC-Cy7 conjugate), CD95 (BUV737 conjugate), followed by intracellular staining with

SIV Gag protein p27 (FITC conjugate, clone 55-2F12, conjugated in-house) and Ki67 (PE-Cy7 conjugate). PrimeFlow RNA assay was carried out according to manufacturer's instructions (Thermo Fisher Scientific). Generally, the SIV specific oligonucleotide target probe set that contains 22~50 pairs could bind to SIV *env*, *gag*, and *pol* mRNA, then signal amplification is achieved through sequential hybridization with multiple amplifier molecules. All data were acquired on BD LSRII flow cytometer and analyzed by FlowJo software (version 9.9.5).

Statistical analysis. All the statistical and graphic analyses were done using GraphPad Prism software (version 7.0). For comparisons between groups, Kruskal–Wallis one-way analysis of variance was applied in the study. Spearman's rank correlation was used to analyze the correlation between variables. *P* values less than 0.05 were considered to be significant in the study.

SUPPLEMENTAL MATERIAL

Supplemental material is available online only.

SUPPLEMENTAL FILE 1, PDF file, 4.4 MB.

ACKNOWLEDGMENTS

We thank Joern Schmitz, Lawrence Tartaglia, Daniel Ram, Venous Hamza, Abishek Chandrashekar, Jingyou Yu for advice, assistance and reagents. We acknowledge support from the NIH (OD024917, AI149670, AI128751, AI129797, AI126603, AI124377, AI164556) and the Ragon Institute of MGH, MIT, and Harvard.

D.H.B., X.H. designed the study and reviewed all data. X.H. performed the immunological assays and analyzed data. M.A. performed the transcriptomic analysis. D.H.B., J.D.V. edited the manuscript. E.B., M.L., J.L. contributed to materials. X.H. and D.H.B. wrote the paper with all coauthors.

The authors had no competing financial interests.

REFERENCES

- Gandhi RT, Chen BK, Straus SE, Dale JK, Lenardo MJ, Baltimore D. 1998. HIV-1 directly kills CD4+ T cells by a Fas-independent mechanism. *J Exp Med* 187:1113–1122. <https://doi.org/10.1084/jem.187.7.1113>.
- Terai C, Kornbluth RS, Pauza CD, Richman DD, Carson DA. 1991. Apoptosis as a mechanism of cell death in cultured T lymphoblasts acutely infected with HIV-1. *J Clin Invest* 87:1710–1715. <https://doi.org/10.1172/JCI115188>.
- Cooper A, Garcia M, Petrovas C, Yamamoto T, Koup RA, Nabel GJ. 2013. HIV-1 causes CD4 cell death through DNA-dependent protein kinase during viral integration. *Nature* 498:376–379. <https://doi.org/10.1038/nature12274>.
- Li Q, Duan L, Estes JD, Ma ZM, Rourke T, Wang Y, Reilly C, Carlis J, Miller CJ, Haase AT. 2005. Peak SIV replication in resting memory CD4+ T cells depletes gut lamina propria CD4+ T cells. *Nature* 434:1148–1152. <https://doi.org/10.1038/nature03513>.
- Meyaard L, Otto SA, Jonker RR, Mijster MJ, Keet RP, Miedema F. 1992. Programmed death of T cells in HIV-1 infection. *Science* 257:217–219. <https://doi.org/10.1126/science.1352911>.
- Muro-Cacho CA, Pantaleo G, Fauci AS. 1995. Analysis of apoptosis in lymph nodes of HIV-infected persons. Intensity of apoptosis correlates with the general state of activation of the lymphoid tissue and not with stage of disease or viral burden. *J Immunol* 154:5555–5566.
- Veazey RS, DeMaria M, Chalifoux LV, Shvets DE, Pauley DR, Knight HL, Rosenzweig M, Johnson RP, Desrosiers RC, Lackner AA. 1998. Gastrointestinal tract as a major site of CD4+ T cell depletion and viral replication in SIV infection. *Science* 280:427–431. <https://doi.org/10.1126/science.280.5362.427>.
- Doitsh G, Galloway NL, Geng X, Yang Z, Monroe KM, Zepeda O, Hunt PW, Hatano H, Sowinski S, Munoz-Arias I, Greene WC. 2014. Cell death by pyroptosis drives CD4 T-cell depletion in HIV-1 infection. *Nature* 505:509–514. <https://doi.org/10.1038/nature12940>.
- Galloway NL, Doitsh G, Monroe KM, Yang Z, Munoz-Arias I, Levy DN, Greene WC. 2015. Cell-to-cell transmission of HIV-1 is required to trigger pyroptotic death of lymphoid-tissue-derived CD4 T cells. *Cell Rep* 12:1555–1563. <https://doi.org/10.1016/j.celrep.2015.08.011>.
- Espert L, Denizot M, Grimaldi M, Robert-Hebmann V, Gay B, Varbanov M, Codogno P, Biard-Piechaczyk M. 2006. Autophagy is involved in T cell death after binding of HIV-1 envelope proteins to CXCR4. *J Clin Invest* 116:2161–2172. <https://doi.org/10.1172/JCI26185>.
- Benveniste O, Flahault A, Rollot F, Elbim C, Estaquier J, Pedron B, Duval X, Dereuddre-Bosquet N, Clayette P, Sterkers G, Simon A, Ameisen JC, Lepert C. 2005. Mechanisms involved in the low-level regeneration of CD4+ cells in HIV-1-infected patients receiving highly active antiretroviral therapy who have prolonged undetectable plasma viral loads. *J Infect Dis* 191:1670–1679. <https://doi.org/10.1086/429670>.
- Kelley CF, Kitchen CM, Hunt PW, Rodriguez B, Hecht FM, Kitahata M, Crane HM, Willig J, Mugavero M, Saag M, Martin JN, Deeks SG. 2009. Incomplete peripheral CD4+ cell count restoration in HIV-infected patients receiving long-term antiretroviral treatment. *Clin Infect Dis* 48:787–794. <https://doi.org/10.1086/597093>.
- Yang X, Su B, Zhang X, Liu Y, Wu H, Zhang T. 2020. Incomplete immune reconstitution in HIV/AIDS patients on antiretroviral therapy: Challenges of immunological non-responders. *J Leukoc Biol* 107:597–612. <https://doi.org/10.1002/JLB.4MR1019-189R>.
- Barouch DH, Ghneim K, Bosche WJ, Li Y, Berkemeier B, Hull M, Bhattacharyya S, Cameron M, Liu J, Smith K, Borducchi E, Cabral C, Peter L, Brinkman A, Shetty M, Li H, Gittens C, Baker C, Wagner W, Lewis MG, Colantonio A, Kang HJ, Li W, Lifson JD, Piatak M, Jr, Sekaly RP. 2016. Rapid inflammasome activation following mucosal SIV infection of Rhesus monkeys. *Cell* 165:656–667. <https://doi.org/10.1016/j.cell.2016.03.021>.
- Picker LJ, Hagen SI, Lum R, Reed-Inderbitzin EF, Daly LM, Sylwester AW, Walker JM, Siess DC, Piatak M, Jr, Wang C, Allison DB, Maino VC, Lifson JD, Kodama T, Axthelm MK. 2004. Insufficient production and tissue delivery of CD4+ memory T cells in rapidly progressive simian immunodeficiency virus infection. *J Exp Med* 200:1299–1314. <https://doi.org/10.1084/jem.20041049>.
- Meythaler M, Pryputniewicz S, Kaur A. 2008. Kinetics of T lymphocyte apoptosis and the cellular immune response in SIVmac239-infected rhesus macaques. *J Med Primatol* 37 Suppl 2:33–45. <https://doi.org/10.1111/j.1600-0684.2008.00323.x>.
- Cumont MC, Diop O, Vaslin B, Elbim C, Viollet L, Monceaux V, Lay S, Silvestri G, Le Grand R, Muller-Trutwin M, Hurtrel B, Estaquier J. 2008. Early divergence in lymphoid tissue apoptosis between pathogenic and non-pathogenic simian immunodeficiency virus infections of nonhuman primates. *J Virol* 82:1175–1184. <https://doi.org/10.1128/JVI.00450-07>.
- Yoshida H, Kong YY, Yoshida R, Elia AJ, Hakem A, Hakem R, Penninger JM, Mak TW. 1998. Apaf1 is required for mitochondrial pathways of apoptosis and brain development. *Cell* 94:739–750. [https://doi.org/10.1016/s0092-8674\(00\)81733-x](https://doi.org/10.1016/s0092-8674(00)81733-x).
- Li LY, Luo X, Wang X. 2001. Endonuclease G is an apoptotic DNase when released from mitochondria. *Nature* 412:95–99. <https://doi.org/10.1038/35083620>.

20. Suzuki Y, Imai Y, Nakayama H, Takahashi K, Takio K, Takahashi R. 2001. A serine protease, HtrA2, is released from the mitochondria and interacts with XIAP, inducing cell death. *Mol Cell* 8:613–621. [https://doi.org/10.1016/s1097-2765\(01\)00341-0](https://doi.org/10.1016/s1097-2765(01)00341-0).
21. Roumier T, Vieira HL, Castedo M, Ferri KF, Boya P, Andreau K, Druillennec S, Joza N, Penninger JM, Roques B, Kroemer G. 2002. The C-terminal moiety of HIV-1 Vpr induces cell death via a caspase-independent mitochondrial pathway. *Cell Death Differ* 9:1212–1219. <https://doi.org/10.1038/sj.cdd.4401089>.
22. Tzifi F, Economopoulou C, Gourgiotis D, Ardavanis A, Papageorgiou S, Scorilas A. 2012. The role of BCL2 family of apoptosis regulator proteins in acute and chronic leukemias. *Adv Hematol* 2012:524308. <https://doi.org/10.1155/2012/524308>.
23. Pawlowski J, Kraft AS. 2000. Bax-induced apoptotic cell death. *Proc Natl Acad Sci U S A* 97:529–531. <https://doi.org/10.1073/pnas.97.2.529>.
24. Lee HL, Pike R, Chong MHA, Vossenkamper A, Warnes G. 2018. Simultaneous flow cytometric immunophenotyping of necroptosis, apoptosis and RIP1-dependent apoptosis. *Methods* 134–135:56–66. <https://doi.org/10.1016/j.jymeth.2017.10.013>.
25. Cheung KT, Sze DM, Chan KH, Leung PH. 2018. Involvement of caspase-4 in IL-1 beta production and pyroptosis in human macrophages during dengue virus infection. *Immunobiology* 223:356–364. <https://doi.org/10.1016/j.imbio.2017.10.044>.
26. Monroe KM, Yang Z, Johnson JR, Geng X, Doitsh G, Krogan NJ, Greene WC. 2014. IFI16 DNA sensor is required for death of lymphoid CD4 T cells abortively infected with HIV. *Science* 343:428–432. <https://doi.org/10.1126/science.1243640>.
27. Mattapallil JJ, Douek DC, Hill B, Nishimura Y, Martin M, Roederer M. 2005. Massive infection and loss of memory CD4+ T cells in multiple tissues during acute SIV infection. *Nature* 434:1093–1097. <https://doi.org/10.1038/nature03501>.
28. Lu W, Demers AJ, Ma F, Kang G, Yuan Z, Wan Y, Li Y, Xu J, Lewis M, Li Q. 2016. Next-generation mRNA sequencing reveals pyroptosis-induced CD4+ T cell death in early simian immunodeficiency virus-infected lymphoid tissues. *J Virol* 90:1080–1087. <https://doi.org/10.1128/JVI.02297-15>.
29. Munoz-Arias I, Doitsh G, Yang Z, Sowinski S, Ruelas D, Greene WC. 2015. Blood-derived CD4 T Cells naturally resist pyroptosis during abortive HIV-1 infection. *Cell Host Microbe* 18:463–470. <https://doi.org/10.1016/j.chom.2015.09.010>.
30. Subramanian A, Tamayo P, Mootha VK, Mukherjee S, Ebert BL, Gillette MA, Paulovich A, Pomeroy SL, Golub TR, Lander ES, Mesirov JP. 2005. Gene set enrichment analysis: a knowledge-based approach for interpreting genome-wide expression profiles. *Proc Natl Acad Sci U S A* 102:15545–15550. <https://doi.org/10.1073/pnas.0506580102>.
31. Mootha VK, Lindgren CM, Eriksson KF, Subramanian A, Sihag S, Lehar J, Puigserver P, Carlsson E, Ridderstrale M, Laurila E, Houstis N, Daly MJ, Patterson N, Mesirov JP, Golub TR, Tamayo P, Spiegelman B, Lander ES, Hirschhorn JN, Altshuler D, Groop LC. 2003. PGC-1alpha-responsive genes involved in oxidative phosphorylation are coordinately downregulated in human diabetes. *Nat Genet* 34:267–273. <https://doi.org/10.1038/ng1180>.